Published in final edited form as:
Ultrasound Med Biol. 2009 February ; 35(2): 319–328. doi:10.1016/j.ultrasmedbio.2008.08.014.

Measurements of Ultrasonic Attenuation Properties of Mid-Gestational Fetal Pig Hearts

Allyson A. Gibson, **Gautam K. Singh**, **Joseph J. Hoffman**, **Achiau Ludomirsky**, and **Mark R. Holland**
Laboratory for Ultrasonics, Washington University, One Brookings Drive, Campus Box 1105, St. Louis, Missouri 63130

Abstract

The objectives of this study were to measure the relative attenuation properties of the left and right ventricles in fetal pig hearts and to compare the spatial variation in attenuation measurements with those observed in previously published backscatter measurements. Approximately 1.0 mm thick, short-axis slices of excised, formalin-fixed heart were examined from 15 mid-gestational fetal pigs using a 50-MHz single-element transducer. Measurements of the attenuation properties demonstrate regional differences in the left and right ventricular myocardium that appear consistent with the previously reported regional differences in apparent integrated backscatter measurements of the same fetal pig hearts. For regions of perpendicular insonification relative to the myofiber orientation, the right ventricular free wall showed larger values for the slope of the attenuation coefficient from 30–60 MHz (1.48 ± 0.22 dB/(cm•MHz) (mean ± SD (standard deviation)) and attenuation coefficient at 45 MHz (46.3 ± 7.3 dB/cm (mean ± SD)) than the left ventricular free wall (1.18 ± 0.24 dB/(cm•MHz) and 37.0 ± 7.9 dB/cm (mean ± SD) for slope of attenuation coefficient and attenuation coefficient at 45 MHz, respectively). This attenuation study supports the hypothesis that intrinsic differences in the myocardium of the left and right ventricles exist in fetal pig hearts at mid-gestation.

Keywords

tissue characterization; attenuation coefficient; slope of attenuation coefficient; fetal echocardiography; heart; myocardium; high-frequency ultrasound

Introduction

Echocardiographic assessment of the developing fetal heart is becoming an important component of overall prenatal care. The ability to characterize intrinsic features of the developing myocardium may aid researchers and clinicians in identifying those fetuses most at risk for developing congenital heart defects, myopathies, or altered myocardial function due to an adverse intrauterine environment. Observed characteristics of fetal echocardiographic images are significantly dependent upon the inherent ultrasonic properties of the developing myocardium. Observed images of the heart depend upon the combined contributions of both the intrinsic ultrasonic *backscatter* and *attenuation* properties of myocardium (Holland et al.

Corresponding Author: Mark R. Holland, Ph.D., Campus Box 1105, Washington University, One Brookings Drive, St. Louis, MO 63130, voice: 314-935-6402, fax: 314-935-5868, email: mrh@wuphys.wustl.edu.

1998; Holland et al. 2005). These ultrasonic properties are largely determined by the detailed viscoelastic and structural properties of myocardial tissue (Insana et al. 1990; Lizzi et al. 1987; O'Brien et al. 1995; O'Donnell et al. 1979; O'Donnell et al. 1981; Oelze et al. 2002; Rose et al. 1995). Hence, a better understanding of the inherent ultrasonic properties of the developing myocardium and their spatial variation may provide new insights into the development of enhanced echocardiography-based methods to assess heart development and aid in prenatal diagnoses of altered growth trajectories.

In a previous study from our laboratory, we reported measurements of the apparent integrated backscatter properties of excised mid-gestational fetal pig hearts (Gibson et al. 2007). This study showed distinct patterns of backscatter in the left and right ventricular free walls that appeared to correlate with the ventricular myoarchitecture associated with the two sides. For ultrasonic insonficiation perpendicular to the transverse plane of the heart, at the mid-papillary level, the largest level of backscatter in the left ventricular free wall was located within the mid-myocardium and regions of decreased apparent backscatter were located subepicardially and subendocardially. The right ventricular free wall showed the largest level of apparent backscatter in a subepicardial band with less apparent backscatter measured in the subendocardial region. Histological analyses of the ultrasonically imaged fetal pig hearts demonstrated the regions of largest backscatter in the ventricular free walls were areas corresponding to perpendicular insonification relative to the circular myofiber orientation. Regions of the ventricular free wall where the predominant myofiber direction was not perpendicular to the ultrasonic beam exhibited smaller levels of backscatter. Furthermore, for those regions of perpendicular insonification relative to the myofiber orientation, it was seen that the level of apparent integrated backscatter for the right ventricular myocardium was larger than that for the left ventricular myocardium. The objectives of the study reported in this paper are to extend the ultrasonic characterization of fetal hearts by measuring the relative attenuation properties of the fetal myocardium and to compare these attenuation measurements with the apparent backscatter measurements.

Our approach was to investigate excised formalin-fixed, mid-gestational fetal pig heart specimens by measuring the ultrasonic properties from a thin slice of the heart. Mid-gestational fetal pig hearts were chosen for this study because the gross structural formation of the heart is complete by this time point, and fetal pigs of this gestational age are similar in gestational age to human fetuses referred for routine diagnostic fetal echocardiographic evaluation at fetal cardiology clinics of other institutions and our center at St. Louis Children's Hospital. The measurements performed in this study focus on the relative attenuation properties of the left ventricular and right ventricular myocardium. Although formalin fixation can affect the absolute level of attenuation and backscatter parameters (Baldwin et al. 2005a; Bamber et al. 1979; Hall et al. 2000a; Takiuchi et al. 2001; van der Steen et al. 1991) the relative differences should be largely preserved.

Methods

Preparation of specimens

Fifteen mid-gestational, formalin-fixed fetal pigs were obtained from Nebraska Scientific Inc. (Omaha, NE, USA) in compliance with approved procedures established by the Animal Studies Committee at Washington University in St. Louis. The heart and humerus bone were harvested from each of the fetal pigs and placed in 10% formalin solution. Thin (approximately 1.0 mm) flat and parallel short-axis cross-sectional specimens of the fetal hearts, representing a transverse plane perpendicular to the long axis of the heart at the mid-papillary level, were prepared using a previously described method (Gibson et al. 2007). The gestational age of each fetal pig was estimated from the length of the humerus bone using a previously described approach (Wrathall et al. 1974). In our study the estimated age of the 15 fetal pigs was 57 ± 3

days (mean ± standard deviation), representing approximately half of the gestational age of a pig (full gestation of a pig is ~120 days).

Acquisition of ultrasonic attenuation data

Measurements of the ultrasonic attenuation properties of the excised fetal heart specimens were obtained using a shadowed-reflector method (Ophir et al. 1984; Verdonk et al. 1996). In this approach, the approximately 1.0 mm-thick fetal heart specimens were mounted on a stainless-steel plate and placed in a custom-designed and constructed water tank. A broadband, 50-MHz center frequency, single-element transducer (6.35 mm diameter, 12.7 mm focus, Panametrics V390; Panametrics Inc., Waltham, MA, USA) with a nominal 60 μm beam width was used to insonify the specimens and measure the specular reflection from the shadowed surface of the stainless-steel plate. The angle of insonification was perpendicular to the cut face of the myocardial slice such that the ultrasonic wave propagated through the entire thickness of each specimen twice. Figure 1 shows a block diagram illustrating the experimental setup and the orientation of the transducer with respect to the myocardial slice. The transducer was used in pulse-echo mode, and data were acquired over the entire specimen, by translating the transmitting/receiving transducer in a C-scan pattern using a Newport XPS motion controller (Newport Corp., Mountain View, CA, USA) in 50 μm steps. The vertical position of the transducer was adjusted to place the focus at the front face of the stainless-steel plate. A Panametrics 5900 pulser/receiver was used in conjunction with a Panametrics 5627RPP-1 remote pulser/preamplifier to drive the transmit of the Panametrics V390 50-MHz transducer and preamplify the reflected signal from the surface of the shadowed stainless-steel plate. The shadowed reflector signal from each interrogated myocardial site was digitized at 625 megasamples-per-second, signal averaged 64 times, and stored as a 2500-point record using a Tektronix 5052B digital oscilloscope with 8-bit digitization (Tektronix Inc., Beaverton, OR, USA). In addition to the tissue-shadowed reflected signals, unshadowed specular reflections from the stainless-steel plate were acquired as reference signals using the same acquisition parameters.

Data Analyses

Each radio-frequency (RF) signal acquired was gated using a 0.67 μs long Tukey window centered on the reflection off the stainless-steel plate. Contributions to the measured signal arising from myocardial backscatter within the gate were small compared to the specularly-reflected signal from the stainless-steel plate and did not significantly affect the measurements. At each site, the power spectrum was calculated from the gated waveform using a fast Fourier transform and the same algorithm was performed on the water-path-only reference signal from the steel plate.

The power spectrum $\mathbf{P_{reference}(f)}$ of the received reference signal can be expressed as

$$P_{reference}(f)=P_0(f)\cdot E_0(f)^2\cdot[\exp(-\alpha_{host}(f)\cdot 2L)]^2\cdot(D_{host}(f))\cdot(R^{Intensity}_{host\rightarrow reflector}) \quad (1)$$

where $\mathbf{P_0(f)}$ is the transmitted power spectrum, $\mathbf{E_0(f)}$ is the frequency response of the transducer and associated electronics, $\boldsymbol{\alpha}_{\mathbf{host}}\mathbf{(f)}$ is the frequency dependent attenuation coefficient of the host medium (water), **L** represents the distance from the transducer to the stainless-steel plate, $\mathbf{D_{host}(f)}$ is the diffraction effects in the host medium, and **R** is the intensity reflection coefficient at the surface of the stainless-steel reflector. Similarly the received power spectrum, $\mathbf{P_{specimen}(f)}$ of the reflector shadowed by the specimen can be written as

$$P_{specimen}(f)=P_{\mathbf{0}}(f)\cdot E_{\mathbf{0}}(f)^{\mathbf{2}}\cdot[\,\mathbf{exp}(-\alpha_{host}(f)\cdot\mathbf{2}(L-\ell))]^{2}\cdot[\,\mathbf{exp}(-\alpha_{specimen}(f)\cdot\mathbf{2}\ell)]^{\mathbf{2}}\cdot(D_{specimen}(f))\cdot(T^{Intensity}_{host\rightarrow specimen})\cdot(R^{Intensity}_{specimen\rightarrow reflecter})\cdot(T^{Intensity}_{specimen\rightarrow host}) \quad (2)$$

in which ℓ represents the specimen thickness, $\boldsymbol{\alpha}_{\mathbf{specimen}}(f)$ is the frequency dependent attenuation coefficient of the specimen, $\mathbf{D}_{\mathbf{specimen}}(f)$ is the diffraction effects in the path including the host and specimen, and **T** represents the intensity transmission coefficients at the interface between the host medium and specimen. Figure 2a shows representative logarithmic power spectra corresponding to a reference signal and specimen signal for one site within the specimen.

A ratio of the linear reference power spectrum (Equation 1) and linear specimen power spectrum (Equation 2) is then used to calculate the total signal loss (TSL) and compensate for the frequency response of the transducer and associated electronics.

$$TSL=\frac{P_{reference}(f)}{P_{specimen}(f)}=[\,\mathbf{exp}(\alpha_{specimen}(f)-\alpha_{host}(f))\cdot\mathbf{2}\ell]^{\mathbf{2}}\cdot\left[\frac{R^{Intensity}_{host\rightarrow reflector}}{(T^{Intensity}_{host\rightarrow specimen})\cdot(R^{Intensity}_{specimen\rightarrow reflector})\cdot(T^{Intensity}_{specimen\rightarrow host})}\right] \quad (3)$$

The total signal loss has contributions arising from the reflection and transmission losses at the water, tissue and stainless-steel interfaces as well as the losses associated with the intrinsic attenuation properties of myocardial tissue. The effects of diffraction are not explicitly stated in the expression for the total signal loss because of the similarity of the velocity of sound in water and myocardium. Furthermore, because the experiment is performed at 50 MHz, the attenuation coefficient of water, the host medium, cannot be neglected. At the experimental temperature of 24°C, the frequency dependent attenuation coefficient of water was taken to be $\boldsymbol{\alpha_{host}(f)} = \mathbf{(2.2\times10^{-4})}\cdot\boldsymbol{f}^{\mathbf{2}}$ $\mathrm{cm}^{-1}\mathrm{MHz}^{-2}$ where f is the frequency in MHz (AIUM 1992).

By rearranging Equation 3 and converting to logarithmic units, the compensated signal loss is written as

$$\alpha_{specimen,dB}(f)\cdot\mathbf{2}\ell=\mathbf{10\log}(P_{reference})-\mathbf{10\log}(P_{specimen})+\alpha_{host,dB}(f)\cdot\mathbf{2}\ell-\mathbf{10\log}\left[\frac{R^{Intensity}_{host\rightarrow reflector}}{(T^{Intensity}_{host\rightarrow specimen})\cdot(R^{Intensity}_{specimen\rightarrow reflector})\cdot(T^{Intensity}_{specimen\rightarrow host})}\right] \quad (4)$$

where $\boldsymbol{\alpha}_{\mathbf{specimen,dB}}(\mathbf{f})$ and $\boldsymbol{\alpha}_{\mathbf{host,dB}}(\mathbf{f})$ are expressed in units of dB/cm and the signal loss due to water (host) is added to the reflection and transmission losses. The reflection and transmission coefficients were calculated based on the acoustic impedance values (MKS units) of stainless steel (45.4 MRayl), water (1.46 MRayl), and fixed myocardium (1.67 MRayl) (Baldwin et al. 2005b; Yang et al. 2006). The value for the acoustic impedance of myocardium was derived from density and speed of sound measurements of fixed ovine myocardium at lower frequencies. However, we anticipate the potential difference in the acoustic impedance for the two species and two frequency ranges should have minimal effects on the reported results. Figure 2b displays representative total signal loss and compensated signal loss curves for one site. After these compensations were applied to the measured signal loss, the attenuation coefficient as a function of frequency was determined by dividing by twice the thickness of the tissue. The tissue thickness was determined with a micrometer that was mounted on the custom-designed cutting tool used to slice the specimens.

The compensated attenuation coefficient was further analyzed to determine the attenuation coefficient at a specific frequency and the frequency dependence of the attenuation coefficient over the usable bandwidth. A line was fit to the compensated attenuation coefficient data over the useful 6 dB bandwidth of 30 MHz to 60 MHz. From this best-fit line the slope of attenuation coefficient and attenuation coefficient at 45 MHz were recorded for each site interrogated. This algorithm was applied to every shadowed reflector RF signal obtained to form images of the entire fetal pig heart slice. Images of the attenuation properties were created by mapping the attenuation measurements to grayscale values and displaying them as pixels in either a slope of attenuation coefficient from 30–60MHz image or an attenuation coefficient at 45 MHz image. Figure 3a displays a representative slope of attenuation image for one of the fetal pig hearts. All data analysis was performed using Igor Pro (WaveMetrics Inc., Portland, OR, USA) on a PowerBook G4 (Apple Inc., Cupertino, CA, USA).

Measurement of attenuation properties from the left ventricular and right ventricular free walls

To compare the attenuation properties of the left ventricular myocardium with those of the right, measurements were obtained from regions of perpendicular insonification relative to the predominant myofiber orientation based on previous analyses of the backscatter data from these fetal hearts (Gibson et al. 2007). These specific regions of interest were chosen to reduce the confounding effects of tissue anisotropy on the ultrasonic measurements and enable assessment of other intrinsic properties of the tissue. Figure 3b illustrates the placement of the regions of interest on a representative slope of attenuation image.

The regions of interest used for analyses in each attenuation image were similar in size, shape, and placement as those regions used previously (Gibson et al. 2007). Each region of interest was centered on a line bisecting the ventricular free walls and septum. The size of the region of interest was uniform within each individual heart, but varied between different hearts depending on the transmural dimension of the regions of perpendicular insonification, as validated by histology. The average area for the regions of interest was 0.533 mm^2. The regions were always chosen to be small enough to cover only the band of perpendicular insonification, but large enough to provide reasonable spatial averaging of measured values. Because the fetal hearts were not repositioned between acquisitions of backscatter and attenuation data, each region of interest was drawn on the backscatter images and copied onto the attenuation images to ensure the same myocardial regions were compared for each heart.

Results

Regional Variation of Attenuation Properties

Parametric images generated from measurements of the slope of the attenuation coefficient from 30–60 MHz and attenuation coefficient at 45 MHz illustrate distinct patterns of attenuation in the left and right ventricular myocardium for all 15 specimens investigated. These spatial variations in attenuation properties are consistent with those reported for apparent integrated backscatter values (Gibson et al. 2007) and are further examined in the *Discussion* section. The attenuation images show distinctly different patterns of values in the left and right ventricular myocardium implying distinct ventricular myoarchitecture and properties between the two sides. In these images the darkest levels, representing relatively small attenuation coefficient or small slope of attenuation coefficient values, are located in the mid-myocardium of left ventricles and brighter regions (higher attenuation coefficient or slope of attenuation coefficient) are located in the subepicardium and subendocardium. Values range from approximately 0.5 dB/(cm•MHz) to 1.5 dB/(cm•MHz) for slope of attenuation coefficient (20 to 60 dB/cm for the attenuation coefficient at 45 MHz) in this region. In the right ventricular myocardium the regions with lower attenuation values were positioned more subepicardially

with regions of higher attenuation values on the endocardial side of the ventricular free wall. Right ventricular values ranged from 1.0 dB/(cm•MHz) to 2.5 dB/(cm•MHz) for slope of attenuation coefficient and 40 to 70 dB/cm for the attenuation coefficient at 45 MHz in this region. Figure 3 shows representative patterns of attenuation for the left and right ventricular myocardium for one of the fetal hearts.

Comparison of attenuation properties

In general, the right ventricular myocardium of each ultrasonic attenuation image exhibits larger values of the slope of attenuation coefficient and the attenuation coefficient at 45 MHz than the left ventricular myocardium. Figure 4 shows the results of attenuation measurements from the left and right ventricular myocardium for regions of perpendicular insonification relative to myofibers. This figure depicts a) measurements of the slope of attenuation coefficient from 30–60 MHz and b) the attenuation coefficient at 45 MHz for the 15 fetal pig hearts along with the corresponding mean levels. In both sets of measurements, the right ventricular myocardium yields significantly larger values than the left ventricular myocardium, both for paired analyses within each specimen ($p < 0.0001$; paired t-test) as well as overall ($p < 0.005$; unpaired t-test; N=15). Specifically, the mean slope of attenuation coefficient over the experimental bandwidth was 1.48 ± 0.22 and 1.18 ± 0.24 dB/(cm•MHz) (mean ± standard deviation; $N = 15$; $p < 0.005$; unpaired t-test) from the myocardium of the right ventricle and left ventricle, respectively. The mean attenuation coefficient at 45 MHz was 46.3 ± 7.3 dB/cm for the right ventricular myocardium and 37.0 ± 7.9 dB/cm for the left ventricular myocardium (mean ± standard deviation; $N = 15$; $p < 0.005$; unpaired t-test) showing a 9.3 dB/cm difference between the two ventricles.

Discussion

Unlike mature adult hearts, both ventricles of fetal hearts are exposed to similar pressures that represent an important determinant of ventricular geometry. Despite the similar prenatal loading conditions, previous embryologic studies suggest the left and right ventricular myocardium develop differently (Salih et al. 2004; Sanchez-Quintana et al. 1995; Smolich et al. 1989). These developmental differences lead to particular interest in quantifying the intrinsic differences in the left and right ventricular myoarchitecture and properties of the developing heart. Because the intrinsic composition and myofiber orientation of the heart can affect measured ultrasonic properties and hence fetal echocardiographic imaging, our aim is to analyze the ultrasonic attenuation parameters and compare these to the reported backscatter results, as a means of characterizing the fetal myocardium.

High frequency analysis of the ventricular myocardium shows transmural variations in the attenuation properties of the heart that appear consistent with the variations observed in previously published backscatter data (Gibson et al. 2007). Grayscale images of the histology, apparent integrated backscatter values, slope of attenuation coefficient values, and attenuation coefficient at 45MHz values are shown in Figure 5 for a representative fetal pig heart specimen. Both the backscatter and attenuation images display bands within the mid-myocardium of the left ventricular free wall and the subepicardial area of the right ventricular free wall that correspond to insonification perpendicular to the predominant myofiber orientation as validated by histology.

The three panels in Figure 6 depict mean transmural line profiles of the apparent integrated backscatter values and slope of attenuation coefficient values for the left ventricular free wall, septal wall, and right ventricular free wall, as well as a pictorial representation of the approximate location of each line profile for each heart investigated. The line profiles for each heart wall were generated by plotting the measured backscatter or attenuation values as a function of the percentage of wall thickness. Results from each specimen were averaged to

produce the mean line profiles illustrated. The line profile data represents that corresponding to the bisecting line for each specimen as indicated in Figure 3b. The nature of the transmural line profiles depicted in Figures 6 appears consistent with what would be anticipated based on previously published studies examining the effects of anisotropy on ultrasonic parameters (Baldwin et al. 2006;Hall et al. 1997;Hoffmeister et al. 1995;Kumar and Mottley 1994;Madaras et al. 1988;Mottley and Miller 1988;Mottley and Miller 1990;Sosnovik et al. 2001;Verdonk et al. 1996). Specifically, these studies demonstrated that maximum values of apparent backscatter with minimum levels of attenuation are associated with perpendicular insonification relative to the myofibers whereas, for non-perpendicular insonification larger levels of attenuation and smaller levels of apparent backscatter are observed. The measured line profiles demonstrate that the maximum apparent integrated backscatter values and slope of attenuation coefficient values are larger in the right ventricular free wall than the corresponding values in the left ventricular free wall.

Comparison of the values in these line profiles with the mean values for the slope of attenuation coefficient depicted in Figure 4 and the backscatter results reported previously (Gibson et al. 2007) demonstrate slight differences. This is a result of averaging the line profiles from the 15 individual hearts, each exhibiting slight variations in transmural myofiber orientation. Hence, the absolute ultrasonic values are somewhat muted by the influence of varying fiber orientation, and the detailed shape of the transmural line profiles may be influenced as well. On average these observed transmural variations of the acoustic properties of the left and right ventricular myocardium are consistent with previously published fiber architecture data. Sanchez-Quintanta *et al.* describe architecture of three layers (subepicardial, middle, subendocardial) in the left ventricular myocardium and a right ventricular fiber architecture consisting of only two layers (subendocardial, subepicardial) for the prenatal and adult human hearts (1995).

Additional insights regarding the intrinsic properties of fetal myocardium can be obtained by further analyses of those regions of perpendicular insonification within the ventricular free walls. A comparison of the ultrasonic measurements in the left and right ventricular regions show both the attenuation coefficient (and its frequency dependence) and the backscatter levels are larger in the right ventricular myocardium than in the left ventricular myocardium. Because the results from these regions (perpendicular insonification) diminish the effects of fiber orientation, these differences may imply compositional differences between the two ventricles. This observation is consistent with previously published data from mature hearts that demonstrate higher collagen content in the right ventricular myocardium compared to the myocardium of the left ventricle (Hoyt et al. 1984; Hoyt et al. 1985). These studies also showed that an increase in myocardial collagen concentration correlates with an increase in both the measured ultrasonic attenuation and backscatter (Hall et al. 2000b; Hoyt et al. 1984; Hoyt et al. 1985; Mimbs et al. 1980; Mimbs et al. 1981; Nguyen et al. 2001; O'Donnell et al. 1979; O'Donnell et al. 1981; Perez et al. 1984; Pohlhammer and O'Brien 1981; Wear et al. 1989; Wong et al. 1993).

Clinical Implications

The results of these ultrasonic measurements of excised fetal hearts permit an assessment of the myoarchitecture and intrinsic properties of the developing heart. Although these measurements obtained at 50 MHz are well beyond the frequencies used clinically, the influence of the regional variations in acoustic properties discernable at high frequencies may affect features observed in clinical fetal echocardiographic imaging (Holland et al. 1998). Previous studies from our laboratory suggest several of the features of myocardial backscatter observed at lower frequencies (e.g., anisotropy of backscatter) (Hoffmeister et al. 1995; Mottley and Miller 1988) are observed at higher frequencies as well (Bridal et al. 1993; Hall et al. 2000a; Hall et al. 2000b; Saijo et al. 1997).

Knowledge of the intrinsic properties of the fetal heart may permit researchers and clinicians to more accurately identify abnormalities of the myocardium earlier than they are currently identified and permit an enhanced interpretation of the *in vivo* examinations of the fetal heart. Congenital heart defects and cardiomyopathies that exhibit a spectrum of pathologic substrates with myocardial fiber disarray and altered myoarchitecture evolve in the first trimester but are only recognized by current echocardiographic modalities in the second trimester. An evaluation of intrinsic properties of the fetal myocardium, discernable by backscatter and attenuation properties in the early stages of hearts destined to develop in congenital heart defects, myopathies or altered myocardial function due to an adverse intrauterine environment, will likely improve diagnostic ability and the scope of favorable intervention in the future.

Limitations

A potential limitation of this study was that ultrasonic measurements were performed on formalin-fixed specimens at room temperature. While it is known that fixation does affect absolute values of ultrasonically measured quantities (Baldwin et al. 2005a; Bamber et al. 1979; Hall et al. 2000a; Takiuchi et al. 2001; van der Steen et al. 1991), the measurements performed in this study focused on relative properties of the heart, which should be largely preserved in fixed myocardium. For this research study, the length of time required for data acquisition (hours) and concerns regarding fresh tissue degradation made the use of fresh tissue impractical, although desirable.

The region of interest placement may represent another concern of our study. Regions of interest were intentionally located in areas primarily perpendicular to the direction of insonification, as validated by histological analysis, in order to minimize the effects of myocardial anisotropy. However, it is possible that some regions encircle a few non-perpendicular fibers. Because the analysis averages over the entire area enclosed, the large number of perpendicular fibers in the enclosed area will minimize the effects of the non-perpendicular fibers.

Summary

Measurements of the attenuation coefficient at 45 MHz and slope of attenuation coefficient from 30–60 MHz demonstrate regional differences between the left and right ventricular myocardium of the developing heart that appear to correspond to previously reported regional differences in apparent integrated backscatter measurements and histological analyses (Gibson et al. 2007). Measurements exhibited the smallest levels of attenuation and the largest levels of backscatter for those regions where insonification was perpendicular to the predominant myofiber direction. More specifically, for data acquired with insonification perpendicular to the cut faces of the transverse cross-sectional fetal heart specimens, lower attenuation values and higher backscatter values were located in the mid-myocardium of the left ventricle and located more subepicardially in the right ventricular myocardium. Furthermore, attenuation and backscatter values for perpendicular insonification in the right ventricular free wall were larger than those areas in the left ventricular free wall, suggesting intrinsic differences between the two ventricles.

The results of this study appear consistent with previously published literature examining the differences in tissue properties of developing hearts (Salih et al. 2004; Sanchez-Quintana et al. 1995; Smolich et al. 1989). It is interesting to note that, in spite of exposure to similar prenatal loading conditions, the left and right ventricular myocardium show architectural and compositional differences in the ultrasonic measurements. This suggests that the left and right ventricles of the fetal heart follow a biogenetically predetermined trajectory of growth and development that may be altered by the intrauterine environment. An adverse environment can result in an altered trajectory of the developing heart leading to a permanent change in

cardiovascular structure and physiology (Barker 1995; Lucas 1991). Hence, prenatal changes in structural and viscoelastic properties resulting in altered ultrasonic properties of the myocardium may permit analyses of fetal echocardiographic images to discern cardiac changes with consequential long-term postnatal effects.

Acknowledgements

We would like to thank Professor James G. Miller, Ph.D. of Washington University in St. Louis for his helpful suggestions regarding this research project.

References

AIUM. Acoustic Output Measurement and Labeling Standard for Diagnostic Ultrasound Equipment. Rockville, MD: American Institute of Ultrasound in Medicine; 1992. American institue of ultrasound in medicine: Standards and technical report.

Baldwin SL, Yang M, Marutyan KR, Wallace KD, Holland MR, Miller JG. Ultrasonic detection of the anisotropy of protein cross-linking in myocardium. IEEE Ultrason Symp 2005a:2263–2266.

Baldwin SL, Yang M, Marutyan KR, Wallace KD, Holland MR, Miller JG. Measurements of the anisotropy of ultrasonic velocity in freshly excised and formalin-fixed myocardial tissue. J Acoust Soc Am 2005b;118:505–513. [PubMed: 16119369]

Baldwin SL, Marutyan KR, Yang M, Wallace KD, Holland MR, Miller JG. Measurements of the anisotropy of ultrasonic attenuation in freshly excised myocardium. J Acoust Soc Am 2006;119:3130–3139. [PubMed: 16708967]

Bamber JC, Hill CR, King JA, Dunn F. Ultrasonic propagation through fixed and unfixed tissues. Ultrasound Med Biol 1979;5:159–165. [PubMed: 388777]

Barker DJ. Fetal origins of coronary heart disease. BMJ 1995;311:171–174. [PubMed: 7613432]

Bridal SL, Recchia D, Miller JG, Wickline SA. Anisotropy of apparent integrated backscatter, signal loss, and backscatter coefficient at 30 to 45 mhz in canine papillary muscle. Ultrason Imaging Tissue Characterization 1993;15:155–156.

Gibson AA, Singh GK, Kulikowska A, Wallace KD, Hoffman JJ, Ludomirsky A, Holland MR. Regional variation in the measured apparent ultrasonic backscatter of mid-gestational fetal pig hearts. Ultrasound Med Biol 2007:1955–1962. [PubMed: 17689180]

Hall CS, Verdonk ED, Wickline SA, Perez JE, Miller JG. Anisotropy of the apparent frequency dependence of backscatter in formalin fixed human myocardium. J Acoust Soc Am 1997;101:563–568. [PubMed: 9000744]

Hall CS, Dent CL, Scott MJ, Wickline SA. High-frequency ultrasound detection of the temporal evolution of protein cross linking in myocardial tissue. IEEE Trans Ultrason Ferroelec Freq Control 2000a; 47:1051–1058.

Hall CS, Scott MJ, Lanza GM, Miller JG, Wickline SA. The extracellular matrix is an important source of ultrasound backscatter from myocardium. J Acoust Soc Am 2000b;107:612–619. [PubMed: 10641669]

Hoffmeister BK, Wong AK, Verdonk ED, Wickline SA, Miller JG. Comparison of the anisotropy of apparent integrated ultrasonic backscatter from fixed human tendon and fixed human myocardium. J Acoust Soc Am 1995;97:1307–1313. [PubMed: 7876450]

Holland MR, Wilkenshoff UM, Finch-Johnston AE, Handley SM, Perez JE, Miller JG. Effects of myocardial fiber orientation in echocardiography: Quantitative measurements and computer simulation of the regional dependence of backscattered ultrasound in the parasternal short-axis view. J Am Soc Echocardiogr 1998;11:929–937. [PubMed: 9804097]

Holland MR, Kovacs A, Posdamer SH, Wallace KD, Miller JG. Anisotropy of apparent backscatter in the short-axis view of mouse hearts. Ultrasound Med Biol 2005;31:1623–1629. [PubMed: 16344125]

Hoyt R, Skorton DJ, Collins SM, Melton HE Jr. Ultrasonic backscatter and collagen in normal ventricular myocardium. Circulation 1984;69:775–782. [PubMed: 6697461]

Hoyt RH, Collins SM, Skorton DJ, Ericksen EE, Conyers D. Assessment of fibrosis in infarcted human hearts by analysis of ultrasonic backscatter. Circulation 1985;71:740–744. [PubMed: 3882268]

Insana MF, Wagner RF, Brown DG, Hall TJ. Describing small-scale structure in random media using pulse-echo ultrasound. J Acoust Soc Am 1990;87:179–192. [PubMed: 2299033]

Kumar KN, Mottley JG. Quantitative modeling of the anisotropy of ultrasonic backscatter from canine myocardium. IEEE Trans Ultrason Ferroelectr Freq Control 1994;41:441–450.

Lizzi FL, Ostromogilsky M, Feleppa EJ, Rorke MC, Yaremko MM. Relationship of ultrasonic spectral parameters to features of tissue microstructure. IEEE Trans Ultrason Ferroelectr Freq Control 1987;34:319–329. [PubMed: 18291854]

Lucas A. Programming by early nutrition in man. Ciba Found Symp 1991;156:38–50. [PubMed: 1855415]discussion 50–35

Madaras EI, Perez J, Sobel BE, Mottley JG, Miller JG. Anisotropy of the ultrasonic backscatter of myocardial tissue: Ii. Measurements in vivo. J Acoust Soc Am 1988;83:762–769. [PubMed: 3351134]

Mimbs JW, O'Donnell M, Bauwens D, Miller JG, Sobel BE. The dependence of ultrasonic attenuation and backscatter on collagen content in dog and rabbit hearts. Circ Res 1980;47:49–58. [PubMed: 6247101]

Mimbs JW, O'Donnell M, Miller JG, Sobel BE. Detection of cardiomyopathic changes induced by doxorubicin based on quantitative analysis of ultrasonic backscatter. Am J Cardiol 1981;47:1056–1060. [PubMed: 7223651]

Mottley JG, Miller JG. Anisotropy of the ultrasonic backscatter of myocardial tissue: I. Theory and measurements in vitro. J Acoust Soc Am 1988;83:755–761. [PubMed: 3351133]

Mottley JG, Miller JG. Anisotropy of the ultrasonic attenuation in soft tissues: Measurements in vitro. J Acoust Soc Am 1990;88:1203–1210. [PubMed: 2229659]

Nguyen CT, Hall CS, Scott MJ, Zhu Q, Marsh J, Wickline SA. Age-related alterations of cardiac tissue microstructure and material properties in fischer 344 rats. Ultrasound Med Biol 2001;27:611–619. [PubMed: 11397525]

O'Brien PD, O'Brien WD Jr, Rhyne TL, Warltier DC, Sagar KB. Relation of ultrasonic backscatter and acoustic propagation properties to myofibrillar length and myocardial thickness. Circulation 1995;91:171–175. [PubMed: 7805199]

O'Donnell M, Mimbs JW, Miller JG. The relationship between collagen and ultrasonic attenuation in myocardial tissue. J Acoust Soc Am 1979;65:512–517. [PubMed: 489819]

O'Donnell M, Mimbs JW, Miller JG. Relationship between collagen and ultrasonic backscatter in myocardial tissue. J Acoust Soc Am 1981;69:580–588. [PubMed: 7462481]

Oelze ML, Zachary JF, O'Brien WD Jr. Characterization of tissue microstructure using ultrasonic backscatter: Theory and technique for optimization using a gaussian form factor. J Acoust Soc Am 2002;112:1202–1211. [PubMed: 12243165]

Ophir J, Shawker TH, Maklad NF, Miller JG, Flax SW, Narayana PA, Jones JP. Attenuation estimation in reflection: Progress and prospects. Ultrasonic Imaging 1984;6:349–395. [PubMed: 6399169]

Perez JE, Barzilai B, Madaras EI, Glueck RM, Saffitz JE, Johnston P, Miller JG, Sobel BE. Applicability of ultrasonic tissue characterization for longitudinal assessment and differentiation of calcification and fibrosis in cardiomyopathy. J Am Coll Cardiol 1984;4:88–95. [PubMed: 6736460]

Pohlhammer J, O'Brien WD Jr. Dependence of the ultrasonic scatter coefficient on collagen concentration in mammalian tissues. J Acoust Soc Am 1981;69:283–285. [PubMed: 7217526]

Rose JH, Kaufmann MR, Wickline SA, Hall CS, Miller JG. A proposed microscopic elastic wave theory for ultrasonic backscatter from myocardial tissue. J Acoust Soc Am 1995;97:656–668. [PubMed: 7860840]

Saijo Y, Tanaka M, Okawai H, Sasaki H, Nitta SI, Dunn F. Ultrasonic tissue characterization of infarcted myocardium by scanning acoustic microscopy. Ultrasound Med Biol 1997;23:77–85. [PubMed: 9080620]

Salih C, McCarthy K, Ho SY. The fibrous matrix of ventricular myocardium in hypoplastic left heart syndrome: A quantitative and qualitative analysis. Ann Thorac Surg 2004;77:36–40. [PubMed: 14726030]

Sanchez-Quintana D, Garcia-Martinez V, Climent V, Hurle JM. Morphological changes in the normal pattern of ventricular myoarchitecture in the developing human heart. Anat Rec 1995;243:483–495. [PubMed: 8597295]

Smolich JJ, Walker AM, Campbell GR, Adamson TM. Left and right ventricular myocardial morphometry in fetal, neonatal, and adult sheep. Am J Physiol 1989;257:H1–9. [PubMed: 2750930]

Sosnovik DE, Baldwin SL, Lewis SH, Holland MR, Miller JG. Transmural variation of myocardial attenuation measured with a clinical imager. Ultrasound Med Biol 2001;27:1643–1650. [PubMed: 11839409]

Takiuchi, S.; Marsh, JN.; Hall, CS.; Lanza, GM.; Wickline, SA. IEEE Ultrason Symp. 2001. Unexpected anisotropic behavior of ultrasound attenuation after collagen cross-linking in porcine tendons.

van der Steen AF, Cuypers MH, Thijssen JM, de Wilde PC. Influence of histochemical preparation on acoustic parameters of liver tissue: A 5-mhz study. Ultrasound Med Biol 1991;17:879–891. [PubMed: 1725228]

Verdonk ED, Hoffmeister BK, Wickline SA, Miller JG. Anisotropy of the slope of ultrasonic attenuation in formalin fixed human myocardium. J Acoust Soc Am 1996;99:3837–3843. [PubMed: 8655813]

Wear KA, Milunski MR, Wickline SA, Perez JE, Sobel BE, Miller JG. Differentiation between acutely ischemic myocardium and zones of completed infarction in dogs on the basis of frequency-dependent backscatter. J Acoust Soc Am 1989;85:2634–2641. [PubMed: 2663954]

Wong AK, Osborn TG, Miller JG, Wickline SA. Quantification of ventricular remodeling in the tight-skin mouse cardiomyopathy with acoustic microscopy. Ultrasound Med Biol 1993;19:365–374. [PubMed: 8356780]

Wrathall A, Bailey J, Hebert C. A radiographic study of development of appendicular skeleton in the fetal pig. Res Vet Sci 1974;17:154–168. [PubMed: 4418908]

Yang M, Baldwin SL, Marutyan KR, Wallace KD, Holland MR, Miller JG. Elastic stiffness coefficients (c11, c33, and c13) for freshly excised and formalin-fixed myocardium from ultrasonic velocity measurements. J Acoust Soc Am 2006;119:1880–1887. [PubMed: 16583926]

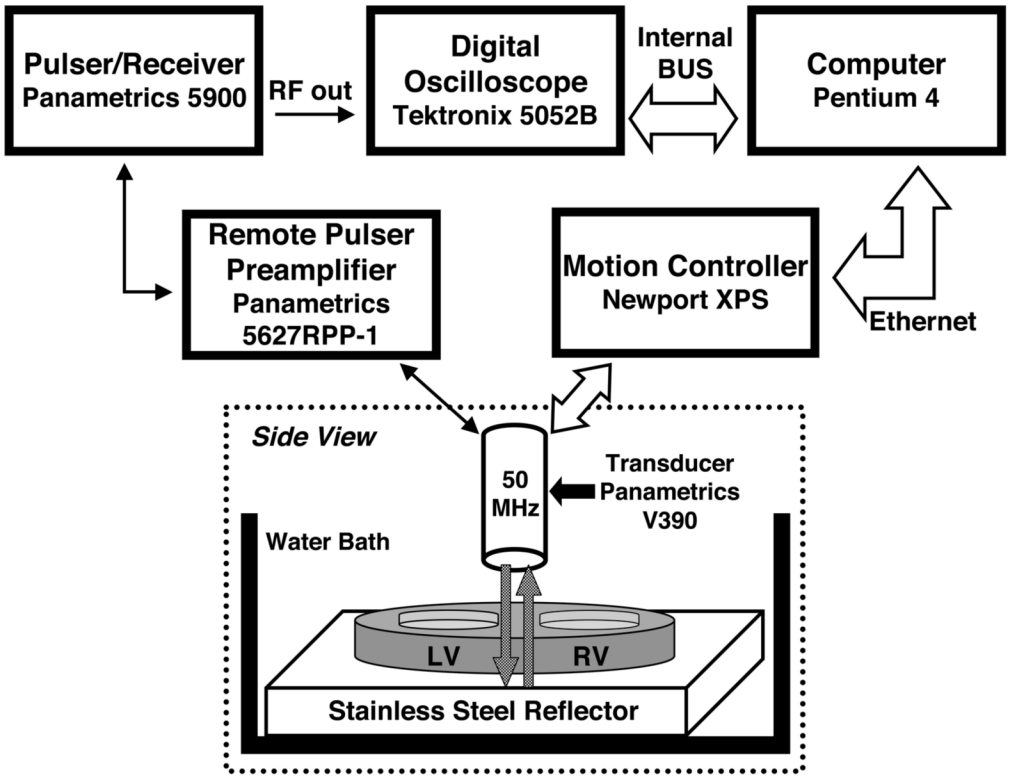

Figure 1.
Block diagram illustrating the experimental setup. The 50-MHz transducer scans the excised heart specimen in a C-scan format. LV=left ventricle; RV=right ventricle

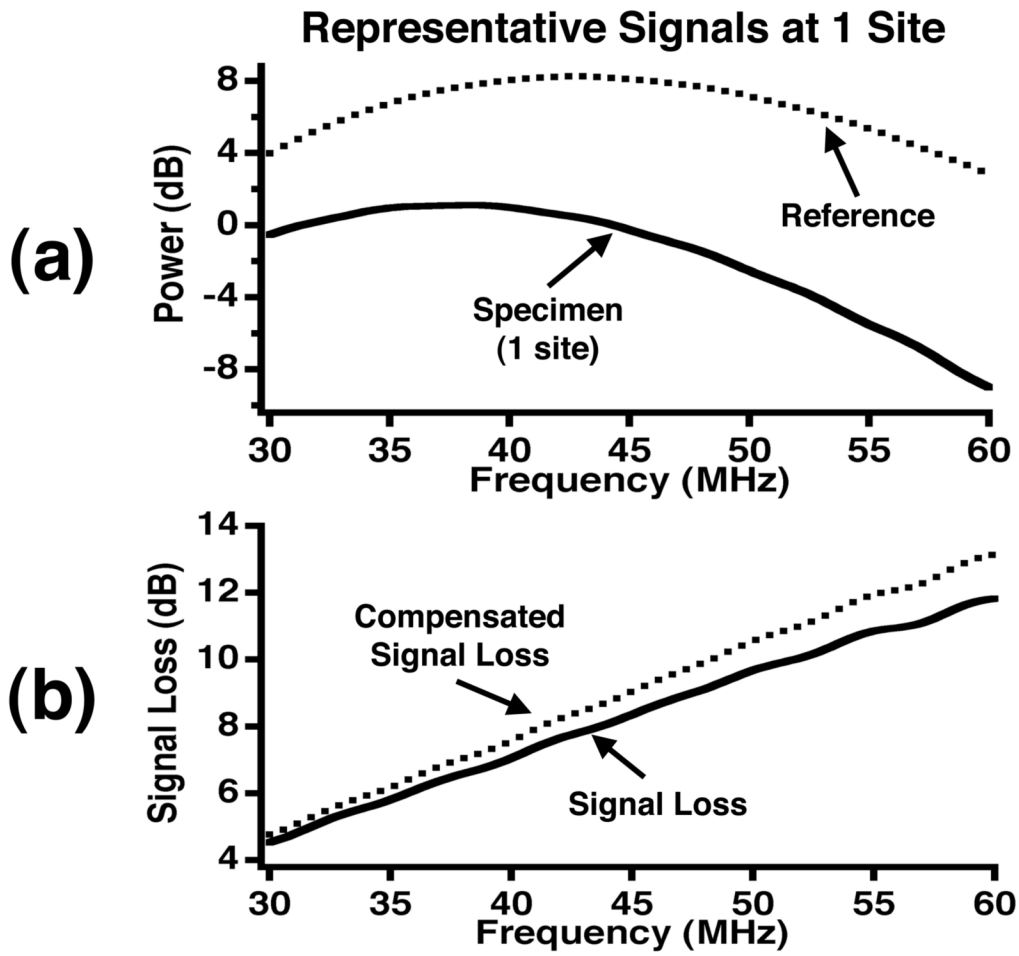

Figure 2.
(a) Representative power spectra for a reference signal and specimen signal at one site. (b) A representative signal loss curve and signal loss compensated for transmission and reflection effects and the attenuation effect of water at high frequencies.

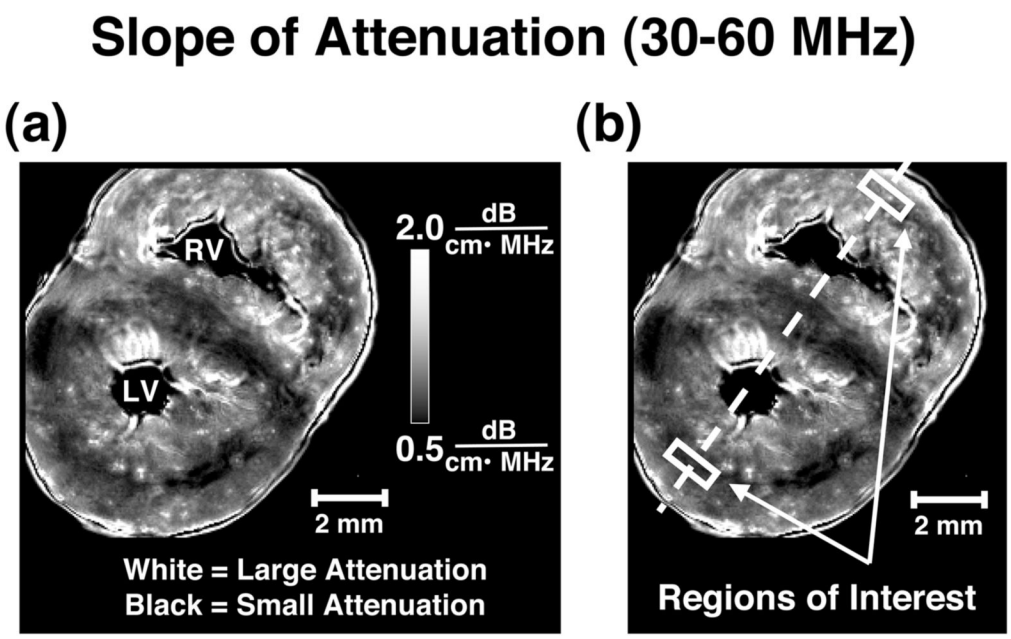

Figure 3.

(a) Representative slope of attenuation image of a fetal pig heart with bright pixels representing relatively large values for slope of attenuation and dark pixels representing small values for slope of attenuation (range 0.5 to 2.0 dB/(cm•MHz)). LV=left ventricle; RV=right ventricle (b) An illustration of the bisecting line used for line profile analysis and locations of the regions of interest in a representative slope of attenuation image.

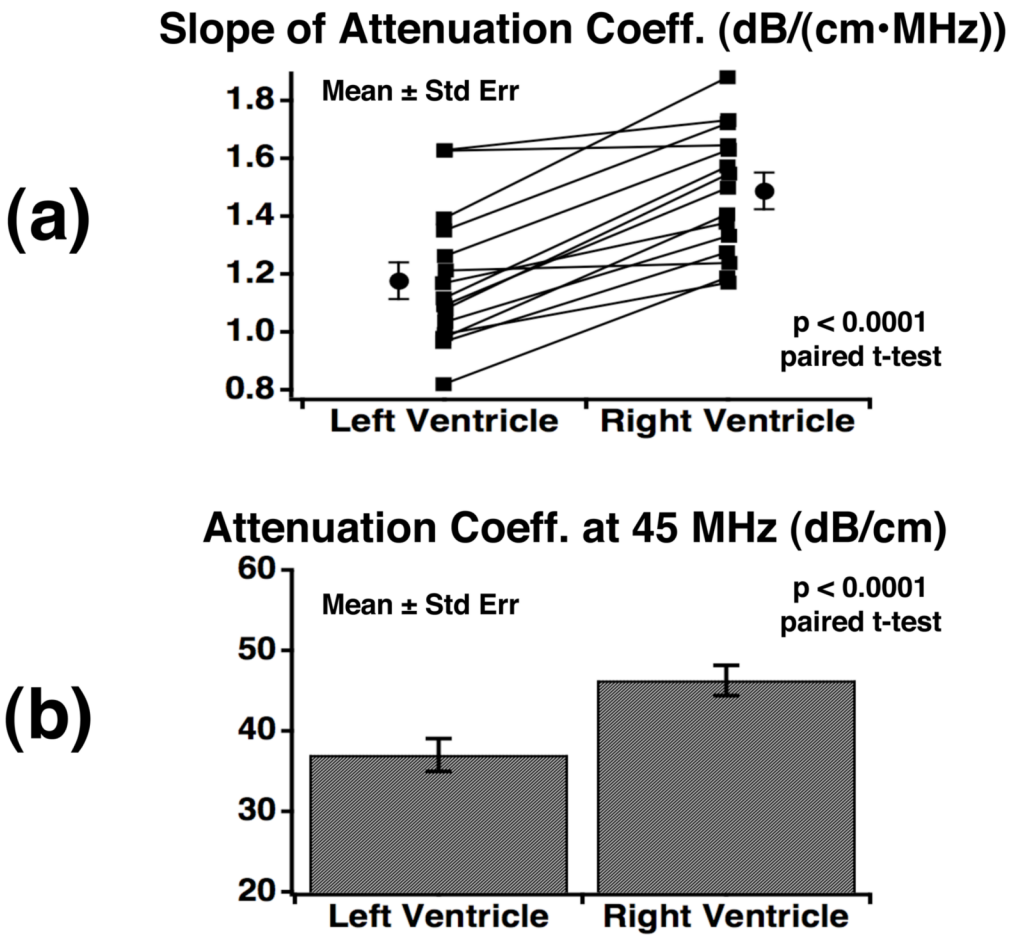

Figure 4.

(a) Individual and mean ± standard error values (N=15) for the slope of attenuation coefficient from regions within the ventricular free walls with perpendicular insonification relative to the predominant myofiber orientation. (b) The mean and standard error (N=15) of the attenuation coefficient at 45 MHz from the left and right ventricular free walls where insonification is perpendicular to the predominant myofiber orienation.

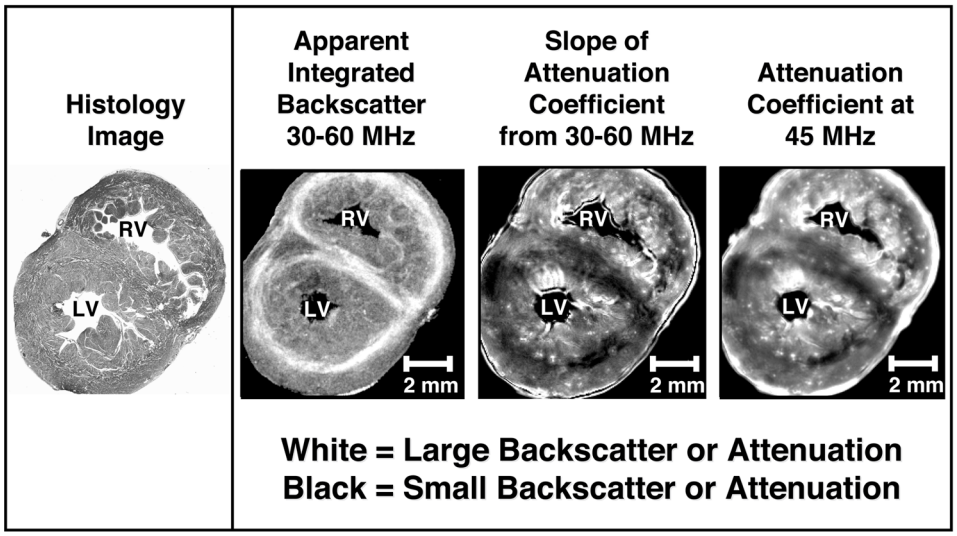

Figure 5.

Histology, backscatter, and attenuation images from a representative fetal pig heart. White represents large apparent integrated backscatter values in the second image from the left and large values for slope of attenuation coefficient and attenuation coefficient at 45 MHz in the two right images, respectively. Black represents small values of apparent integrated backscatter in the second image and small slope of attenuation coefficient and attenuation coefficient at 45 MHz values in the two right images. LV=left ventricle; RV=right ventricle

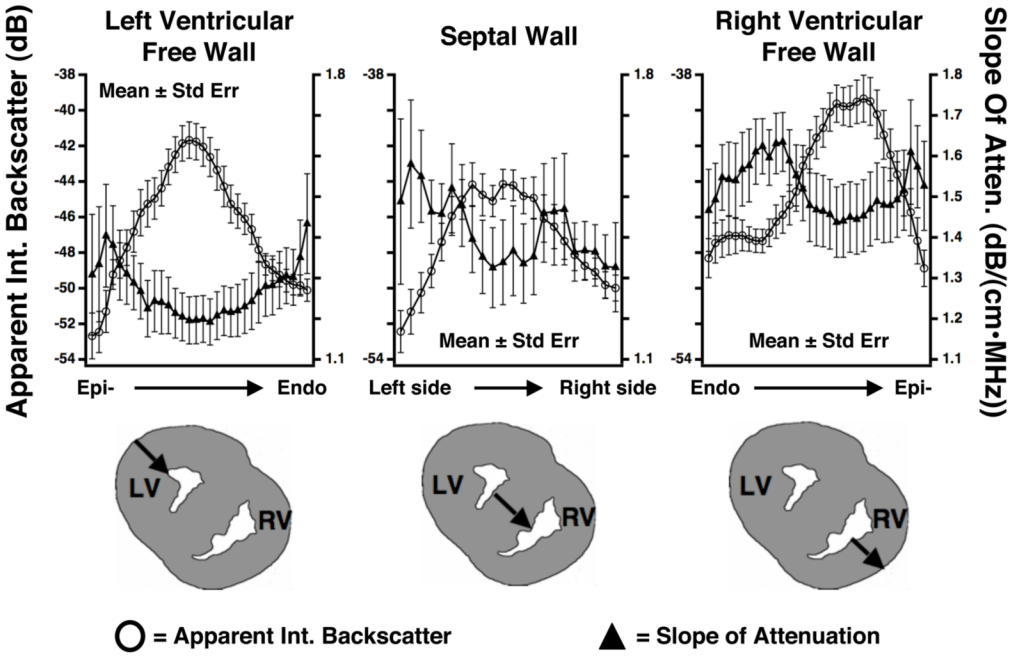

Figure 6.

Mean (± SE) values of the apparent integrated backscatter (IBS) and slope of attenuation coefficient with respect to position within the left ventricular free wall, septal wall, and right ventricular free wall for 15 fetal pig heart specimens. The open circles represent average apparent integrated backscatter values and correspond to the left axes. The average slope of attenuation coefficient values are plotted using triangles and correspond to the right axes. Below the graphs are illustrations of the locations of the line profiles within the walls of the fetal pig hearts. LV=left ventricle; RV=right ventricle